

Quantum Sensing of Intermittent Stochastic Signals

Sara L. Mouradian,¹ Neil Glikin,¹ Eli Megidish,¹ Kai-Isaak Ellers,¹ and Hartmut Haeflner¹

¹*Physics Department, University of California, Berkeley, California 94720, USA*

An ideal quantum sensor would comprise a large ensemble of quantum systems with uniform high fidelity control and readout (F), but experimental demonstrations face a trade-off between these parameters. We investigate how the number of sensors and fidelity affect sensitivity for a range of signals. We consider estimation of the variance and frequency of stochastic signals. For continuous signals we find that increasing the number of sensors by $1/F^2$ for $F < 1$ recovers the sensitivity achievable when $F = 1$. However, there is a stronger dependence on F when the signal is intermittent. We demonstrate this with a single trapped ion sensor to highlight the importance of high fidelity control and reaching the quantum projection noise limit.

Quantum metrology aims to estimate a physical parameter of a signal via the response of a controllable quantum sensor coupled to the signal. Ideally, entanglement between quantum sensors can be exploited to break classical sensing limits [1], but even without entanglement, quantum systems can reach the quantum projection noise (QPN) limit [2] — a noise floor unattainable by classical systems. Quantum sensors have been used to demonstrate state-of-the-art amplitude [3, 4] and frequency estimation [5–9]. The figure of merit for a quantum sensor depends on the application and here we focus on a sensor’s sensitivity — the minimum parameter that can be accurately resolved — which depends on the response of the sensor to the parameter of interest and the noise on the measurement of the sensor’s state. An ideal quantum sensor would comprise a large number (M) of individual quantum systems with a long ensemble coherence time and unity fidelity state preparation, control, and measurement across the ensemble. However, an experimental implementation must balance the gain in sensitivity due to increased M with any potential loss in fidelity due to increased decoherence or non-uniform control [10]. This trade-off is well studied for constant and coherent signals, but many signals of interest are stochastic with a finite autocorrelation time. Moreover, some signals of interest are intermittent [11], such as in astronomy [12, 13], which places strict restrictions on the maximum integration time for each individual measurement and thus the signal which can be obtained.

In this manuscript, we investigate how a sensor’s sensitivity scales with M and F for four signals of interest illustrated in Fig. 1(b-e): (1) Amplitude estimation of a constant signal (Sec. I A); (2) Variance estimation of the amplitude of a 0-mean stochastic signal (Sec. I B); (3) Frequency estimation of a two-frequency stochastic signal (Sec. II A); and (4) frequency estimation of an *intermittent* two-frequency stochastic signal (Sec. II B). The stochastic signals all have an autocorrelation time longer than each individual Ramsey integration time, (t_i), but shorter than the total measurement time (t_{meas}) comprising N individual integration periods plus the additional time needed for state preparation and measurement (see Fig. 1(a)).

We estimate a parameter g of a field $B(g, t)$ via a Ram-

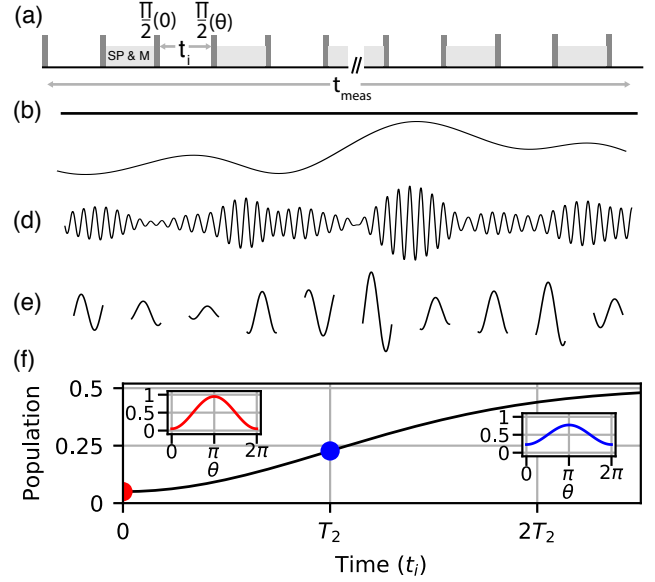


FIG. 1. (a) Depiction of the Ramsey sequence used for sensing including the time needed for state preparation and measurement (SP and M). The phase θ of the second $\pi/2$ pulse is chosen to optimize the sensitivity to the parameter of interest. (b-e) The signals considered in this manuscript. (b) A constant amplitude signal. (c) A stochastic signal. (d) A two-frequency stochastic signal. (e) An intermittent two-frequency stochastic signal. (f) A Ramsey signal with increasing t_i with no signal applied with population $p = 0.5(1 - C(t))$. Insets show the reduced contrast at $t = 0$ — dominated by sub-unity state preparation, operations, and measurement — and at the T_2 time of the sensor — dominated by decoherence.

sey measurement as depicted in Fig. 1(a) [14]. N projective measurements of the population (p) of M sensors are used to estimate the phase ($\phi(g, t_i)$) accrued by the sensor due to $B(g, t)$ during an individual integration time t_i . The interferometer is biased with an added phase θ to optimize the response to the parameter of interest. The M sensors are unentangled such that the noise on the population measurement is bounded below by the QPN, $\sigma_{\text{qpn}}^2 = p(1 - p)/(NM)$.

Errors in state-preparation, control, and measurement contribute to a time-independent sub-unity fidelity F .

Decoherence due to coupling to the environment reduces the maximum achievable contrast over time such that $C(t) = Fe^{-\chi(t)}$ with a known function $\chi(t)$. Here we assume that the coherence of the sensor is limited by slow noise and the contrast exhibits a Gaussian decay, characterized by a coherence time T_2 , $\chi(t) = \frac{t^2}{2T_2^2}$. Fig. 1(f) plots $p(0, t) = 0.5(1 - C(t))$ for a sensor with $F = 0.9$ and an arbitrary T_2 time.

With the field applied, the population is $p(g, t) = \frac{1}{2} [1 - C(t) \cos(\theta + \phi(g, t))]$. The sensor's signal is then the change in final population, $\Delta p(g, t) = p(g, t) - p(0, t)$ due to the parameter of interest (g), and the noise is bounded by the QPN at $p(g, t)$.

The sensitivity is the parameter g_{\min} for which the signal-to-noise ratio (SNR) is equal to 1 [14]. For each of the signals above we consider the effect of F on sensitivity and find the number of sensors with sub-unity fidelity that are needed to recover the sensitivity achievable with a single $F = 1$ sensor.

I. AMPLITUDE ESTIMATION

A. A Coherent Signal

We begin with the well-studied case of amplitude estimation of a signal $B(g, t) = g$, such that $\phi(g, t) = gt$. The optimal SNR is obtained by biasing the measurement at $\theta = \pi/2$ so that $p(0, t) = 0.5$ [14]. Small deviations from the bias point due to g will give a sensor response $\Delta p(g, t) \approx \frac{1}{2}C(t)gt$. The QPN is to first order unaffected by the presence of the signal. The minimum detectable g is

$$g_{\min} = (\sqrt{NM}t_i C(t_i))^{-1}. \quad (1)$$

which is optimized at $t_i = T_2$. In Fig. 2 it is clear that non-unity fidelity reduces the achievable sensitivity, but that this can be corrected for using $M = 1/F^2$ sensors. This is a familiar result [14], and state-of-the-art amplitude estimation demonstrations leverage large ensembles to improve the sensitivity while sacrificing contrast [10] as large ensembles of quantum sensors are found naturally in solid state systems [15] or atomic vapor cells [16].

B. A Stochastic Signal

Now we consider variance estimation of a slowly varying stochastic signal with a mean $\langle B \rangle = 0$ and variance $\langle B^2 \rangle = g^2$. The average population of the sensor with the signal applied is

$$\langle p(g, t) \rangle = \frac{1}{2} \left(1 - C(t) \cos(\theta) e^{-g^2 t^2 / 2} \right). \quad (2)$$

The signal adds an additional effective source of decoherence, $1/T_{2, \text{eff}}^2 = 1/T_2^2 + g^2$. Thus, it is advantageous to

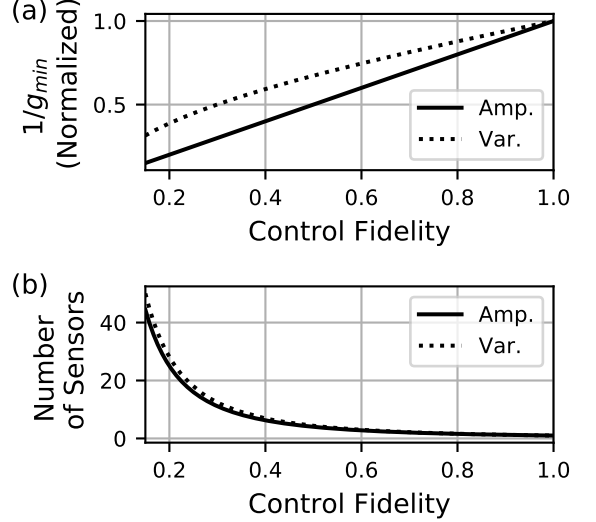


FIG. 2. Comparison between amplitude (solid) and variance (dotted) estimation. (a) The effect of sensor fidelity on the achievable sensitivity for a fixed number of sensors. (b) The number of sensors needed to achieve the same sensitivity as a single unity-fidelity sensor.

bias the measurement at $\theta = 0, \pi$ such that $p(0, t)$ measures the full contrast without the signal applied, and $p(g, t)$ reflects any reduction in contrast due to g . Then, $\Delta p(g, t) = \frac{1}{2}C(t)(1 - e^{-g^2 t^2 / 2})$ and the QPN varies with g a well. Thus, for small g the SNR is

$$\text{SNR} = \frac{\sqrt{NM}C(t)g^2 t^2}{2\sqrt{1 - C^2(t) + C^2(t)g^2 t^2}}, \quad (3)$$

and setting $\text{SNR}=1$ and solving for g , we find

$$g_{\min} = \sqrt{\frac{2C(t_i) + 2\sqrt{C(t_i)^2 + (1 - C(t_i)^2)NM}}{NM C(t_i) t_i^2}}. \quad (4)$$

which is optimized at $t_i \sim \sqrt{2}T_2$. As shown in Fig. 2(a), the scaling of sensitivity with fidelity for variance estimation ($\sim 1/\sqrt{F}$) differs from the scaling for amplitude estimation ($1/F$). However, the scaling with M for variance and amplitude estimation ($\sim 1/\sqrt[4]{M}$, $1/\sqrt{M}$ respectively) changes in step such that $M \simeq 1/F^2$ sensors still nearly compensate for $F < 1$ as seen in Fig. 2(b). Thus, when building a quantum sensor for variance detection it is again best to increase M if the subsequent decrease in F is more modest than $1/\sqrt{M}$.

II. FREQUENCY ESTIMATION

In this section, we consider frequency resolution of a two-frequency stochastic signal. Here we consider a two-frequency signal (Fig. 1(d)) with a finite auto-correlation

time that, as in Sec. IB, is longer than t_i but much shorter than t_{meas} [11] of the form

$$B(t) = A_1 \sin \omega_1 t + B_1 \cos \omega_1 t + A_2 \sin \omega_2 t + B_2 \cos \omega_2 t \quad (5)$$

We describe this signal with three parameters: the frequency separation $g = \omega_1 - \omega_2$, the center frequency $\omega_s = (\omega_1 + \omega_2)/2$, and σ^2 , the variance of the 0-mean normal distribution that describes all four amplitudes $A_{1,2}$, $B_{1,2}$. We assume prior knowledge of ω_s and σ and estimate the frequency separation, g . If ω_s and σ are not previously known, multivariate estimation techniques can be used [11, 17].

A similar estimation problem has been considered in the spatial domain [18, 19], and sub-Rayleigh discrimination of the position of two incoherent light sources has been demonstrated [20, 21]. This method has also been used in conjunction with sum-frequency generation to achieve discrimination between optical frequency and temporal modes [22].

A. A Stochastic Signal

For arbitrary measurement times, we consider the problem numerically for a signal as described in Eq. 5 with $\omega_s = 2\pi \times 1$ kHz and $\sigma = 2\pi \times 500$ Hz with $N = 1000$ measurements of 1 sensor. As for variance estimation, we are measuring an additional time-dependent decoherence due to the signal so the measurement should be biased at $\theta = 0, \pi$ to measure the full contrast.

In Fig. 3(a) we plot $\text{SNR}(t_i)$ for $g = 2\pi \times 10$ Hz which is locally maximized at integer multiples of the center frequency, $t_n = 2\pi n/\omega_s$ with an optimal SNR near $\sqrt{2}T_2$ as indicated by the blue marker in Fig. 3(a). In Fig. 3(b,c) we see that frequency estimation of a stochastic signal scales similarly to variance estimation with respect to M and F . Again, it is optimal to prioritize increasing M over increasing F if the subsequent decrease in F scales more favorably than $1/\sqrt{M}$.

B. An Intermittent, Stochastic Signal

Finally, we consider an intermittent, stochastic two-frequency signal as in Fig. 1(e). In contrast to Sec. II A, the intermittent signal has individual durations less than T_2 , such that each integration time is limited by the signal duration. The signal for frequency estimation approaches 0 for short measurement times, suggesting that frequency estimation is impossible in this scenario. However, a recent proposal [11] claims that a quantum sensor can be used for frequency estimation even for these short measurement times by taking advantage of the scaling of QPN near an eigenstate. As in Sec. IB, II A, we bias the measurement to measure the decrease in contrast due to the signal. However, unlike the previous sections, $t_i \ll T_2$ so the sensor is near an eigenstate as illustrated

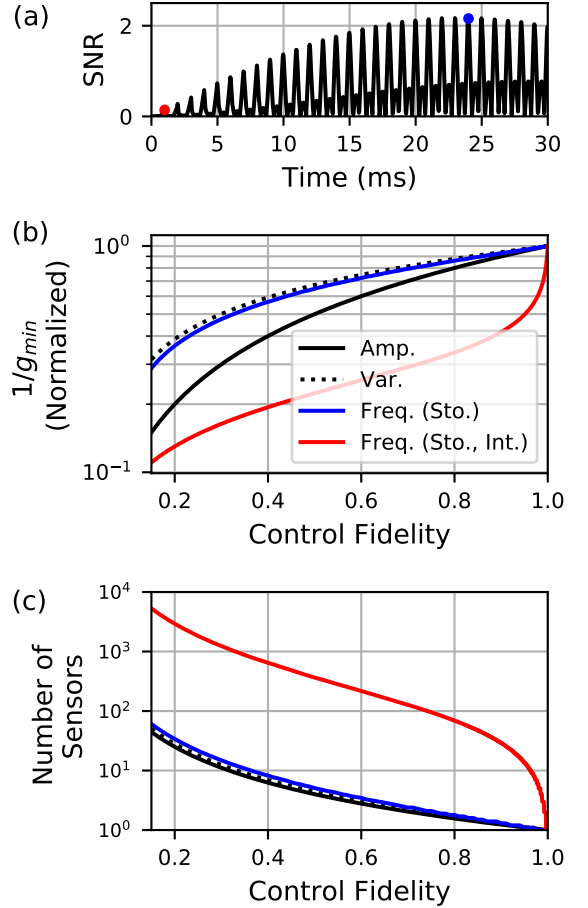


FIG. 3. Frequency estimation of Eq. 5 with $\omega_s = 2\pi \times 1$ kHz, $\sigma = 2\pi \times 500$ Hz, $N = 1000$, $M = 1$. (a) Time dependence of the SNR for frequency estimation of a $g = 2\pi \times 10$ Hz signal. (b) The effect of sensor fidelity on the achievable sensitivity for amplitude and variance estimation (black solid, dotted) and frequency estimation of stochastic continuous (blue) and intermittent (red) signals. (c) The number of sensors needed to achieve the same sensitivity as single unity-fidelity sensor. The color scheme is the same as in (b).

in Fig. 1(f), and it is possible to take full advantage of the fact that QPN approaches 0 for $p = 0, 1$. Thus we recover a finite sensitivity to g [11].

In Sec. II A we found that performing the measurement at $t_n = 2\pi n/\omega_s$ is optimal. In this section, we consider only measurements at $t_1 = 2\pi/\omega_s$ (the red marker in Fig. 3(a)). For signals with longer durations, the optimal sensing procedure is discussed in Ref. [11]. If $g = 0$, an ideal quantum sensor will be in an eigenstate at t_1 . Any non-0 g will lead to dephasing of the probe and for $g \ll \omega_s$,

$$p(g) = \frac{1}{2} \left(1 - C_t e^{-\frac{4\pi^2 \sigma^2}{\omega_s^4} g^2} \right) \approx \frac{1}{2} \left(1 - C_t + C_t \frac{4\pi^2 \sigma^2}{\omega_s^4} g^2 \right). \quad (6)$$

where $C_t = C(t_1)$. Finding the SNR and solving for g

with $\text{SNR}=1$, we find

$$g_{\min} = \frac{\omega_s^2}{2\pi\sigma} \sqrt{\frac{C_t + \sqrt{C_t^2 + NM(1 - C_t^2)}}{NMC_t}}. \quad (7)$$

The red curve in Fig. 3(b) shows a strong departure from the scaling of sensitivity with sensor fidelity seen in the previous sections. This arises because the QPN decreases rapidly towards 0 as the system approaches an eigenstate. This reasoning only holds if the fidelity is near one and the measurement is limited by QPN. Thus, for $F \sim 1$, the scaling of the sensor's sensitivity deviates strongly from the $\sim \sqrt{F}$ scaling found for the sensitivity for frequency or variance estimation of continuous signals. For low F , $M \sim (1/F^2)(1/(1 - e^{-2\chi(t_1)}))$ which is the same scaling as the previous cases, but with a factor which increases rapidly for $t_1 \ll T_2$.

Unlike the previous cases considered, significantly more sensors are necessary to recover the sensitivity achieved with a single unity fidelity sensor as seen in Fig. 3(c) and it is important to retain near-unity fidelity as M is increased. This is in direct contrast to the scalings for parameter estimation of continuous signals. Here we have modeled parameters (described in Sec. II A) that are relevant for the present experiment, but the effect of $F < 1$ will be even stronger for signals with shorter durations — or sensors with longer coherence times. For instance, if $t_1/T_2 = 10^{-3}$, $M \sim 10^6(1/F^2)$ for low F . In this case it will be necessary to have even higher control fidelities while remaining at the QPN limit.

III. EXPERIMENTAL DEMONSTRATION

Finally, we present the first experimental demonstration of quantum sensing of an intermittent signal. Our quantum sensor is a $^{40}\text{Ca}^+$ ion. Specifically, we use the electronic ground state $|S\rangle \equiv ^2\text{S}_{1/2}$, and the long-lived metastable state, $|D\rangle \equiv ^2\text{D}_{5/2}$ in a Ramsey interferometry measurement. The sensor's state is detected via resonant excitation of a cycling state-dependent transition. The number of photons detected during the detection time is thresholded to infer whether the detection event corresponded to the ion in the $|S\rangle$ or $|D\rangle$ state. This is repeated over N measurements, each with a different value of the coefficients of the intermittent signal defined in Eq. 5, obtaining a measurement of $\langle p \rangle$.

We implement the intermittent signal we want to sense with an ac stark shift on the $|S\rangle$ to $|D\rangle$ sensing transition. To do this, an arbitrary waveform generator modulates an rf source driving an acousto-optical modulator controlling the amplitude of laser light detuned 250 kHz from the sensing transition and focused onto the ion. The amplitude of the signal is limited by the available optical power and achievable modulation depth. We use a Hahn-Echo sequence with the signal on only during the first half to remove the effect of the dc bias and any slowly varying noise. The measurement phase (θ) of the

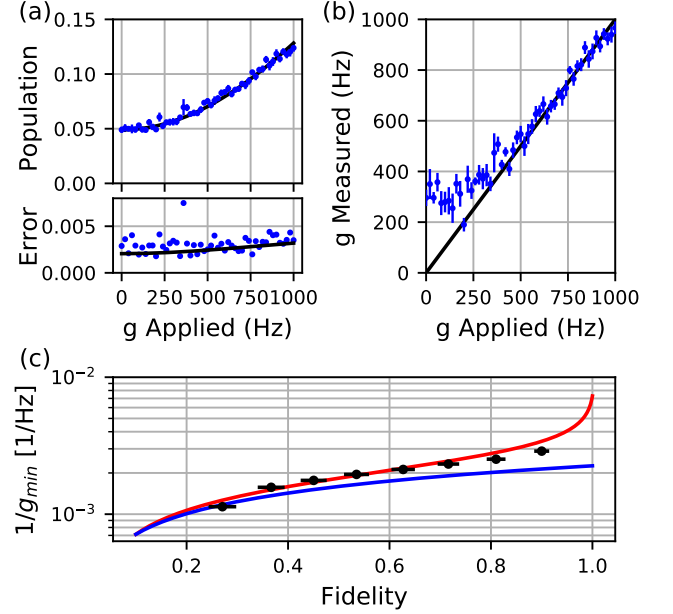


FIG. 4. (a) Population as a function of frequency separation for $\omega_s = 2\pi \times 2$ kHz, $\sigma = 2\pi \times 275$ Hz and the error over 11 sets of $N = 1000$ measurements ($M = 1$) compared to the error expected from QPN. (b) Estimation of the applied frequency separation, g from the population data. (c) Comparison between the experimentally derived sensitivity and the theoretical scalings for intermittent (red) and continuous (blue) stochastic signals.

second $\pi/2$ pulse is chosen such that the sensor is as close as possible to an eigenstate when $g = 0$ to optimize the sensitivity as described in Sec. II B. A phase scan at $g = 0$ bounds the contrast ($C = 0.903 \pm 0.015$) at the given measurement parameters due to the sensor decoherence ($T_2 = 7.97 \pm 0.51$ ms) and control fidelity ($F = 0.91 \pm 0.015$).

We consider the response of our trapped ion sensor to varying frequency separations g for a signal with $\omega_s = 2\pi \times 2$ kHz and $\sigma = 2\pi \times 275$ Hz. Fig. 4(a) shows the increase in population (or decrease in contrast) as g increases. The error is the standard error of 11 repetitions of $N = 1000$ measurements of $M = 1$ sensors. A comparison between the standard error over those 11 repetitions and the error expected from QPN (Fig. 4(a), bottom panel) shows that our noise is nearly dominated by QPN, with 17% excess uncorrelated noise at $g = 0$.

We estimate g using Eq. 6 for each of the 11 measurements of $p(g)$. For $g < g_{\min}$, nearly half of the measurements fall below $p(g = 0) = 0.047$. For these measurements, an estimation of g via Eq. 6 is undefined and thus we disregard them. Fig. 4(b) shows the results of the frequency estimation. For $g > g_{\min}$, the estimated g matches the applied value, while the estimation is biased for $g < g_{\min}$. We use this to extract an experimentally derived g_{\min} . We verify this method with numerical simulations which fit the analytical expression of Eq. 7. For

an intermittent, stochastic 2 kHz signal with individual integration times of only 0.5 ms and a total measurement time of 500 ms we expect to achieve a 290 Hz sensitivity. Experimentally we find only a 346 Hz sensitivity. This discrepancy is due to the noise above the QPN limit and underlines the importance of reaching the QPN limit in the sensing of intermittent signals.

Finally, in order to demonstrate the strong dependence on sensor fidelity laid out in Sec. II B, we post-process our data to artificially reduce the effective contrast of our measurement and derive an empirical g_{\min} as detailed above. In Fig. 4(c) we find that the scaling with contrast matches our expectations (red), and clearly deviates from the $1/\sqrt{F}$ scaling expected for a continuous signal (blue). For instance, a sensor comprising 100 unentangled quantum sensors with $F = F_0/10 = 0.091$ would only be able to resolve a 430 Hz signal and recover the same sensitivity we would need 500 sensors.

IV. CONCLUSION

We have compared variance and frequency estimation of stochastic signals to the familiar case of amplitude detection. We find that for continuous signals, sub-unity control fidelity is easily compensated for with a modest ensemble of sensors. However, if the signal is intermittent, near-unity control fidelity and measurements at

the QPN limit are significantly more important and the number of sensors needed to recover the same sensitivity increases significantly. This manuscript has focused on a specific intermittent signal, but similar results are expected for more general intermittent signals. Experimental implementations of quantum sensing have historically focused on increasing the number of sensors in an ensemble. However, here we show that this is not sufficient if the integration time is limited by the signal and not the sensor's coherence time. Thus it is important to continue optimizing the control fidelity of quantum sensors and to achieve the QPN limit when adding more sensors.

ACKNOWLEDGMENTS

We thank Alex Retzker and Soonwon Choi for valuable conversations during the preparation of this manuscript. S.M. was supported by an appointment to the Intelligence Community Postdoctoral Research Fellowship Program at University of California, Berkeley, administered by Oak Ridge Institute for Science and Education through an interagency agreement between the U.S. Department of Energy and the Office of the Director of National Intelligence. This work has been supported by the ARO MURI grant W911NF-18-1-0218. The apparatus has been supported by ONR through Grant No. N00014-17-1-2278 and by the NSF Grant No. PHY 1620838.

-
- [1] V. Giovannetti, S. Lloyd, and L. Maccone, *Nat. Photonics* **5**, 222 (2011).
 - [2] W. M. Itano, J. C. Bergquist, J. J. Bollinger, J. M. Gilligan, D. J. Heinzen, F. L. Moore, M. G. Raizen, and D. J. Wineland, *Phys. Rev. A* **47**, 3554 (1993).
 - [3] J. M. Taylor, P. Cappellaro, L. Childress, L. Jiang, D. Budker, P. R. Hemmer, A. Yacoby, R. Walsworth, and M. D. Lukin, *Nat. Phys.* **4**, 810 (2008).
 - [4] C. A. Meriles, L. Jiang, G. Goldstein, J. S. Hodges, J. Maze, M. D. Lukin, and P. Cappellaro, *J. Chem. Phys.* **133**, 124105 (2010).
 - [5] G. A. Álvarez and D. Suter, *Phys. Rev. Lett.* **107**, 230501 (2011).
 - [6] T. Yuge, S. Sasaki, and Y. Hirayama, *Phys. Rev. Lett.* **107**, 170504 (2011).
 - [7] L. M. Norris, G. A. Paz-Silva, and L. Viola, *Phys. Rev. Lett.* **116**, 150503 (2016).
 - [8] J. Bylander, S. Gustavsson, F. Yan, F. Yoshihara, K. Harrabi, G. Fitch, D. G. Cory, Y. Nakamura, J.-S. Tsai, and W. D. Oliver, *Nat. Phys.* **7**, 565 (2011).
 - [9] A. Laraoui, J. S. Hodges, and C. A. Meriles, *Appl. Phys. Lett.* **97**, 143104 (2010).
 - [10] J. F. Barry, J. M. Schloss, E. Bauch, M. J. Turner, C. A. Hart, L. M. Pham, and R. L. Walsworth, *Rev. Mod. Phys.* **92**, 015004 (2020).
 - [11] T. Gefen, A. Rotem, and A. Retzker, *Nat. Commun.* **10**, 1 (2019).
 - [12] A. G. Lyne, in *Neutron Stars and Pulsars* (Springer, Berlin, Heidelberg, 2009) pp. 67–72.
 - [13] R. H. Gray, *Int. J. Astrobiol.* **19**, 299 (2020).
 - [14] C. L. Degen, F. Reinhard, and P. Cappellaro, *Rev. Mod. Phys.* **89**, 035002 (2017).
 - [15] H. Clevenson, M. E. Trusheim, C. Teale, T. Schröder, D. Braje, and D. Englund, *Nat. Phys.* **11**, 393 (2015).
 - [16] D. Budker and M. Romalis, *Nat. Phys.* **3**, 227 (2007).
 - [17] R. Demkowicz-Dobrzanski, W. Gorecki, and M. Guta, *J. Phys. A: Math. Theor.* (2020), 10.1088/1751-8121/ab8ef3.
 - [18] C. Lupo and S. Pirandola, *Phys. Rev. Lett.* **117**, 190802 (2016).
 - [19] M. Tsang, R. Nair, and X.-M. Lu, *Phys. Rev. X* **6**, 031033 (2016).
 - [20] W.-K. Tham, H. Ferretti, and A. M. Steinberg, *Phys. Rev. Lett.* **118**, 070801 (2017).
 - [21] R. Nair and M. Tsang, *Phys. Rev. Lett.* **117**, 190801 (2016).
 - [22] J. M. Donohue, V. Ansari, J. Řeháček, Z. Hradil, B. Stoklasa, M. Paúr, L. L. Sánchez-Soto, and C. Silberhorn, *Phys. Rev. Lett.* **121**, 090501 (2018).